International Research Journal of Engineering and Technology (IRJET) e-ISSN: 2395-0056
Volume: 08 Issue: 05 | May 2021 www.irjet.net p-ISSN: 2395-0072

Synthesis, Spectroscopic Investigation of (FT-IR, NMR, UV) and Molecular Docking Study on-3.-(4-Methoxyphenyl) -1-(4-Chlorophenyl)Prop-2-Ene-1-one. Using Quantum Chemical Calculations

Dr. P. Chakkaravarthy., M.Sc,M.Phil.,Ph.D [1]*

*[1]*Department of Chemistry, Government Thirumagal Mills College Gudiyattam, India*

ABSTRACT: The compound of -3-(4-methoxy phenyl)-1-(4-chloro phenyl) prop-2-ene-1-one (4MCPO) was synthesized and characterized by FT-IR, UV-Visible, ^{1}HNMRand ^{13}CNMR spectra. The optimized molecular geometry (bond length, bond angle), the complete vibrational frequency , the infrared intensities calculated by using density functional theory (DFT) B3LYP method with the help of 6-311++G(d,p) basis set. The ^{1}H and ^{13}C nuclear magnetic resonance (NMR) chemical shifts of the molecule are calculated by the gauge-independent atomic orbital (GIAO) method and compared with experimental results. The calculated HOMO and LUMO energies confirm that charge transfer occurs within the molecule. On the basis of the thermodynamic properties of 4MCPO at different temperature have been calculated, revealing the correlation between standard heat capacities (C) standard entropies (S) and standard enthalpy changes (H) and temperatures. DFT calculation of molecular electrostatic potentials (MEP) was carried out at the B3LYP/6-311G (d,p) level of theory. Mullikan population analysis on atomic charges is also calculated. In addition DFT global chemical reactivity descriptors (chemical hardness, total energy, electronic chemical potential and electrophilicity) are calculated for 4MCPO and used to predict their relative stability and reactivity. All the calculations were carried out by B3LYP/6-311G (d,p) method. . The antibacterial and anti fungal activity of the compound was also tested against various pathogens. The molecular docking studies concede that title compound may exhibit 3QNJ inhibitor activity.

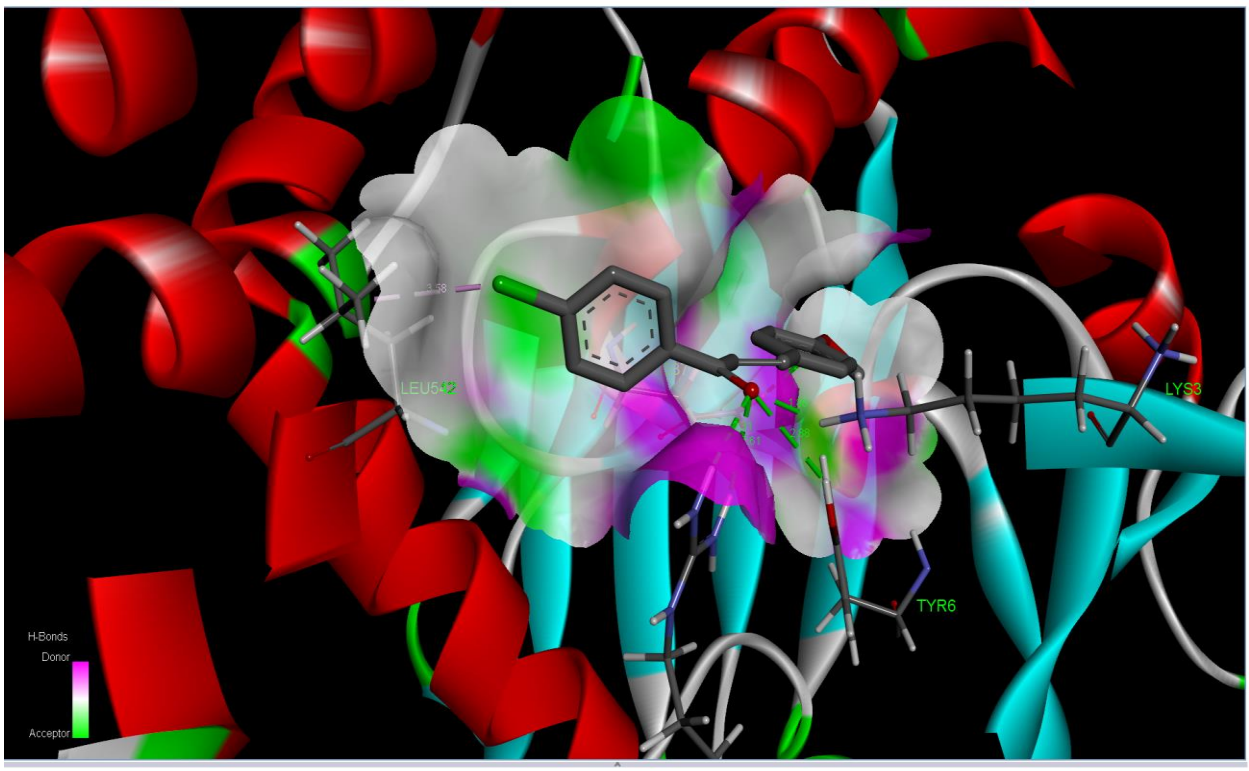

Keywords: FT-IR; DFT;NLO; NBO; Antimicrobial; Molecular docking;.

1 Introduction

Chalcones are an important class of natural compounds and have been widely applied as synthons in synthetic organic chemistry. The nonlinear optical properties of the different chalcone derivatives have been reported [1-4]. These, α,β-unsaturated ketones possess a wide variety of biological activities, including anti-leishmanial [5], anticancer [6, 7], anti-invasive [8], anti-tuberculosis [9], antimicrobial [10,11], antimalarial [12], antitumor [13,14], anti-proliferative [15] and anti-oxidant activity [16]. In addition to their applications in medicinal chemistry, they have recently been explored as molecules with nonlinear optical and luminescent properties [17].

This implies an understanding at the atomic level of the molecular structure of the exposed surfaces of their reactivity and the bonding mechanism. To this extent, quantum chemical calculations have shown the unrivalled capability to elucidate at the atomistic level the mechanism of many phenomena involving surface reactivity. Finally, a recent combined FTIR, UV, NMR and DFT investigation illustrate that the molecular structure, stability and reactivity of 4MCPO atomic sites exposed by Electrostatic potential surfaces exhibit significantly various Lewis acidity and optical power, probably resulting in various reactivity toward chalcone derivative compound.

2 Materials and Methods

2.1 Synthesis

A mixture of the 4-chloro acetophenone (0.01 mole) and 4-methoxy benzaldehyde (0.01 mole) were dissolved in 50 mL of ethanol. Then 15 mL of 10% (0.02 mole) potassium hydroxide (KOH) solution was added drop wise were mixed and stirred at room temperature around 18 hours. The reaction mixture is poured into crushed ice and acidified with dil. HCl (1:1) by drop by drop. The resulting solid (chalcone) was collected by filtration, dried and purified by recrystallisation from acetic acid. The purity of the compounds was confirmed by TLC. The scheme of the synthesis is shown in Fig.1.

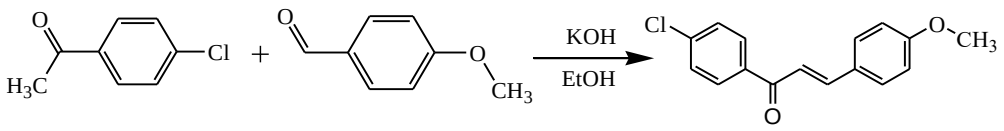

4-Chloro acetophenone 4-Methoxy benzaldehyde 3-(4-Methoxyphenyl)-1-(4-chlorophenyl) prop-2-ene-1-one

Fig.1. The scheme of the synthesis of 4MCPO

2.2 Experimental

The FT-IR spectrum of the synthesis compound 1- (4-Chlorophenyl) -3- Methoxyphenyl) prop-2-em-1-one (4MCPO) was recorded in the region 4000-450 cm^{-1} in evacuation mode using a KBr pellet technique with 1.0 cm^{-1} resolution on a PERKIN ELMER FT-IR spectrophotometer. Carbon (^{13}C) NMR and Proton (^{1}H) NMR spectra were recorded in DMSO-d_6 using TMS as an internal standard on a Bruker high-resolution NMR spectrometer at 400 MHz at CAS in Crystallography & Biophysics, University of Madras, Chennai, India. The ultraviolet absorption spectrum of the sample is examined in the range 250-600 nm using UV-1700 series recording spectrometer.

2.3 Computational details

Entire theoretical calculations were executed with Gaussian 09 program package [18] has been used to calculate optimized molecular geometry, vibrational wavenumbers and NLO activity using DFT/B3LYP method with the 6-311++G(d,p) basis set. To avoid the systematic errors caused by basis set incompleteness, negligence of electron correlation and vibrational anharmonicity a general scaling factor of 0.9461was used to scale the computed wavenumbers. Additionally, the compute vibrational frequencies were revealed by means of the potential energy distribution (PED) investigation of all the fundamental vibration modes by using VEDA 4 program [10] used in previous studies by many researchers [19-21]. NBO 3.1 program was implemented for natural bonding orbital calculation [22]. In order to

understand the electronic properties, the theoretical UV-Vis spectra have been investigated by TD-DFT method with 6-311++G(d,p) basis set for the DMSO. The proton and carbon NMR chemical shift were calculated with the gauge-including atomic orbital (GIAO) approach by applying B3LYP/6-311++G(d,p) method of the title molecule and compared with the experimental NMR spectra. Molecular docking (ligand-protein) simulations have been performed by using auto Dock 4.2.6 software package.

3 Results and Discussion

3.1 Molecular geometry

The optimized structure parameters of 4MCPO were calculated by DFT-B3LYP/6-311++ G(d,p) levels The molecular structure along with numbering of atoms of 4MCPO is obtained from 09W and Gauss View 5.0 programs are shown in Fig.2. The bond parameters (bond length and bond angles) of the 4MCPO molecule is listed in Table .1 using DFT/B3LYP method with 6-311++G(d,p) basis set. Therefore, the crystal data of a closely related molecule such as A monoclinic polymorph of 1-(4-chlorophenyl)-3-(4-methoxyphenyl) prop-2-en-1-one [23] is compared with that of the title compound. This title molecule has seventeen C-C bond lengths, thirteen C-H bond lengths, two O-C bond length, one C-Cl bond length respectively As shown in Fig.2, two aromatic rings are connected through α, β-unsaturated carbonyl which is the main chalcone moiety [24]. Therefore by considering Table.1 and Fig.2. C1-C2 single bond and C1=O4 double bond lengths (exp./cal.) were found as 1.481/1.482Å and 1.2240/1.228Å, respectively. Furthermore, the C2=C3 double bond length (exp./cal.) was found as 1.339/1.348Å and these values are in a good agreement with the calculated values. For the other bond lengths, we can state that there is a good agreement between the observed and calculated values. However, the largest difference between the calculated and experimental values is 0.98Å for the C-H bond lengths of a methyl group at the end of the chain. On the other hand, as presented in Table.1, the C2-C1-O4, C6-C7-H23 and C8-C7-H23 bond angles (exp./cal.) were found as 114.8/115.6,120.6/120.7 and 120.6/120.2 respectively. The presence of a good agreement between the observed and calculated values for the other bond angles can be clearly expressed.

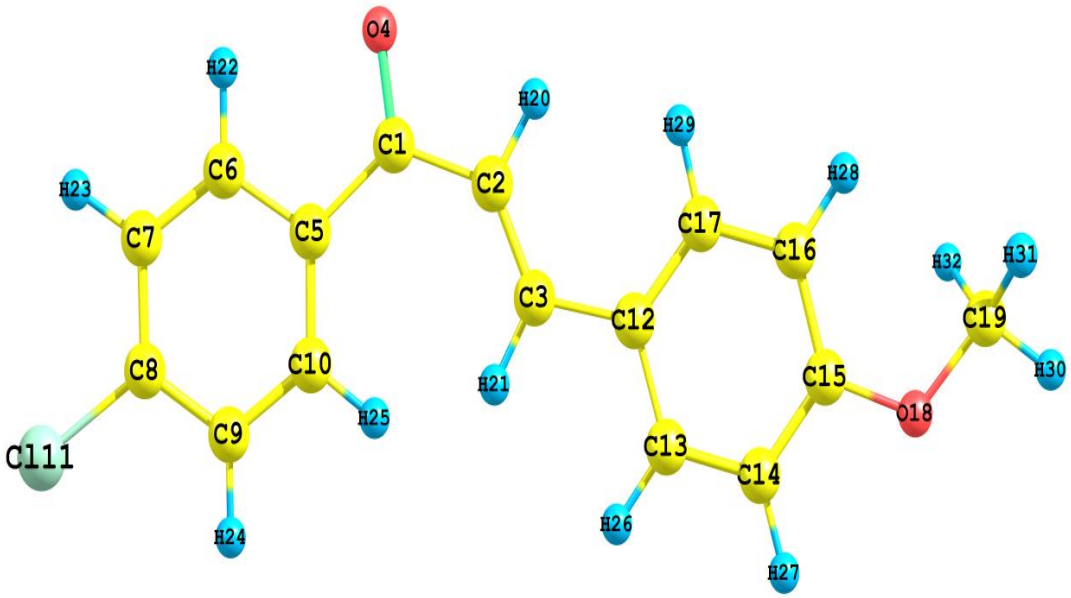

Fig. 2. Optimized geometric structure with atoms numbering of 4MCPO

Table 1 Geometrical parameters optimized in 1-(4-chlorophenyl)-3-(4-methoxyphenyl) prop-2-en-1-one bond length (Å) and bond angle (°) with 6-311++G(d,P) basis set.

Atoms	Experimental[a]	B3LYP/ 6-311++G(d,p)	Atoms	Experimental[a]	B3LYP/6-311++G(d,p)
	Bond length(A^0)			Bond angles(A^0)	
C1-C2	1.481	1.482	C2-C1-O4	114.8	115.6
C1-O4	1.224	1.228	C2-C1-C5	118.3	126.9
C1-C5	1.5	1.514	C1-C2-C3	119.5	133
C2-C3	1.339	1.348	C2-C1-H20	120.2	108.6
C2-H20	0.95	1.086	O4-C1-C5	119.9	117.5
C3-C12	1.464	1.462	C1-C5-C6	118	115.7
C3-H21	0.95	1.081	C1-C5-C10	122.5	126.8
C5-C6	1.401	1.405	C3-C2-H20	116.2	118.5
C5-C10	1.401	1.401	C2-C3-C12	121.4	126.4
C6-C7	1.394	1.388	C2-C3-H21	116.2	120.6
C6-H22	0.95	1.082	C12-C3-H21	116.2	113
C7-C8	1.392	1.392	C3-C12-C13	123.25	118.7
C7-H23	0.95	1.083	C3-C12-C17	118.7	124
C8-C9	1.386	1.389	C6-C5-C10	119.3	117.6
C8-Cl11	1.743	1.756	C5-C6-C7	120.6	121.8
C9-C10	1.339	1.393	C5-C6-H22	119.7	118

C9-H24	0.95	1.082	C5-C10-C9	120.4	121.4
C10-H25	0.95	1.077	C5-C10-H25	119.8	121.6
C12-C13	1.404	1.409	C7-C6-H22	119.7	120.2
C12-C17	1.403	1.403	C6-C7-C8	118.8	119.1
C13-C14	1.391	1.383	C6-C7-H23	120.6	120.7
C13-H26	0.95	1.085	C8-C7-H23	120.6	120.2
C14-C15	1.404	1.4	C7-C8-C9	121.7	120.8
C14-H27	0.95	1.083	C7-C8-Cl11	119.2	119.6
C15-C16	1.403	1.401	C9-C8-Cl11	119.1	119.6
C15-O18	1.365	1.358	C8-C9-C10	118.9	119.3
C16-C17	1.395	1.389	C8-C9-H24	120.5	120.2
C16-H28	0.95	1.082	C10-C9-H24	120.5	120.5
C17-H29	0.95	1.083	C9-C10-H25	120.5	117
C18-C19	1.424	1.424	C13-C12-C17	118	117.3
C19-H30	0.98	1.088	C12-C13-C17	121.1	121.8
C19-H31	0.98	1.095	C12-C13-H26	119.5	119.2
C19-H32	0.98	1.095	C12-C17-C16	121.4	121.7
			C12-C17-H29	120.1	120.1
			C14-C13-H26	119.5	119
			C13-C14-C15	119.5	119.9
			C13-C14-H27	120.2	121.4
			C15-C14-H27	120.2	118.7
			C14-C15-C16	120.15	119.4

	C14-C15-O18	116.2	116
	C16-C15-O18	125.02	124.6
	C15-C16-C17	119.1	119.9
	C15-C16-H28	120.1	120.9
	C15-O18-C19	118	119
	C17-C16-H28	120.1	119.2
	C16-C17-H29	120.1	118.2
	O18-C19-H30	109.5	105.7
	O18-C19-H31	109.5	111.3
	O18-C19-H32	109.5	111.3
	H30-C19-H31	109.5	109.4
	H30-C19-H32	109.5	109.4
	H31-C19-H32	109.5	109.7

[a] Taken from Ref [23]

3.2 Vibrational Analysis

The title molecule consists of 32 atoms, which has 90 modes of vibrations. The vibrational frequencies are calculated using the scaling factor 0.9641 for B3LYP/6-311++G (d,p) levels. Based on the normal modes of analysis vibrational assignments are made. The theoretical and experimental frequencies are harmonized using the above scaling factors and the values are presented in Table.2. The theoretical and experimental IR spectrum of 4MCPO is represented in Fig.3.

3.2.1 C-H Vibrations

In the aromatic compounds, the C-H stretching wave numbers appear in the range 3000-3100 cm^{-1} which are the characteristic region for the ready identification of molecule C-H stretching vibrations [25]. The C-H stretching and bending regions are of the most difficult regions to interpret in infrared spectra. The nature and position of the substituent cannot affect these vibrations. the aromatic compounds have almost four infrared peaks in the region 3080- 3010 cm^{-1} due to ring C-H stretching bands [26]. In this present study, the C-H stretching vibrations are observed at 3086,3038,3036,3033,3026,3024,3023,3013,2993,2988,2928,2907 and 2849cm^{-1} [Mode no's 1-13] by B3LYP/6-311++G(d,P) method show good agreements with experimental vibrations. The bands observed in the recorded FT-IR spectrum 3084(s), 3034(s) 2926(m) and 2843(s) cm^{-1}. The PED corresponding to this pure mode of title molecule contributed 98, 100, 95, 88, 79, 91, 80, 94, 92, 94, 90, 100, and 92% is shown in Table.2.

The bands due to the in-plane C-H bending vibrations are observed in the region of 1000–1300 cm^{-1} [27,28].The in-plane C-H bending vibrations are calculated to be in the range 1438-971cm^{-1} (mode nos: 21 to 28, 31, 32, 34, 35, 36, 37, 38, 39, 40, 41, 45) for 4MCPO.. These modes are observed in the FTIR: 1438(S), 1419(m), 1313(m), 1238(m), 1184(w) 1130(m), 1093(m), 1058(m), cm^{-1} spectra with weak intensity. with PED contribution 59, 70, 74, 71, 23, 21, 38, 31, 34, 25, 10, 34, 11, 27, 27, 28, 33, 54, and 10 % respectively. In FT-IR Spectrum This also shows good agreement, experiment recorded data.

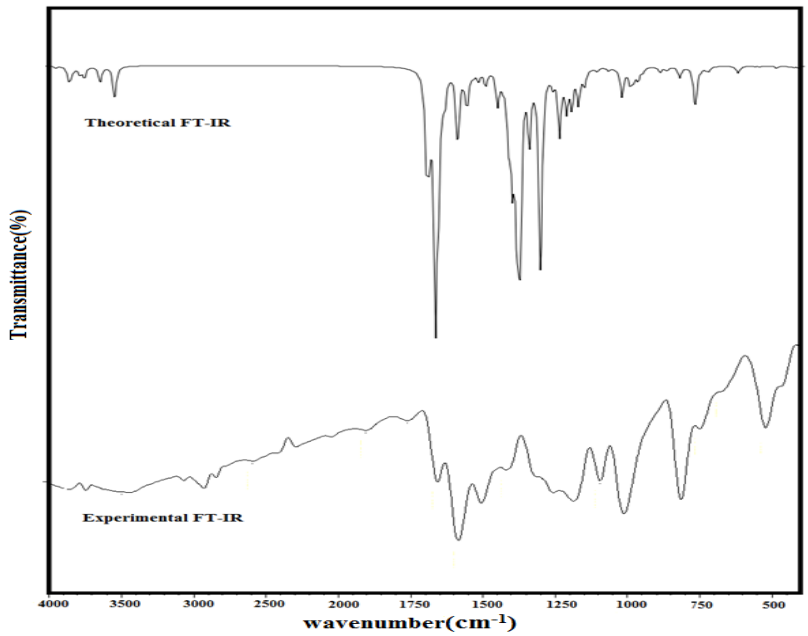

Fig. 3. FT- IR spectra of 4MCPO. (Experimental, B3LYP/6-311++G(d,p))

Table.2 Observed and calculated frequencies of 4MCPO at a B3LYP method with 6-311++G(d,p) basis set

Mode No	Experimental wavenumber (cm^{-1})	Theoretical Wavenumber (cm^{-1})				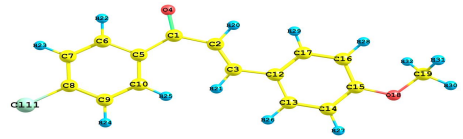
	FTIR	Unscaled	Scaled[b]	IR^{C}_{int}	I_{RAMAN}[d]	Assignments (PED)[a]
1	3084(m)	3262	3086	1	0	StrCH(98)
2	3034(s)	3211	3038	1	3	StrCH(100)
3		3206	3033	0	4	StrCH(95)
4		3208	3036	4	2	StrCH(88)
5		3198	3026	1	1	StrCH(79)
6		3196	3024	1	2	StrCH(91)
7		3195	3023	0	4	StrCH(80)
8		3185	3013	1	2	StrCH(94)
9		3163	2993	1	0	StrCH(92)
10		3158	2988	2	1	StrCH(94)
11	2926(m)	3094	2928	4	2	StrCH(90)
12		3073	2907	7	4	StrCH(100)
13	2843(s)	3011	2849	14	2	Str CH(92)
14	1666(m)	1763	1668	29	5	Str CC(48)bend HCC(12)
15	1583(s)	1676	1586	24	33	StrOC(72)
16		1638	1550	100	1	StrCC(24)
17		1624	1536	33	100	StrCC(56)
18		1603	1516	1	8	StrCC(49)
19	1504(m)	1598	1512	8	1	StrCC(46)
20		1544	1460	30	14	StrCC(10)+bendHCC(51)

21	1438(s)	1517	1435	2	2	StrCC(10)+bendHCC(59)
22		1504	1423	13	1	bendHCH(70)+TorsHCOC(22_)
23	1419(m)	1498	1418	2	1	bendHCH(74)+TorsHCOC(17)
24		1476	1397	2	0	bendHCH(71)
25		1454	1376	4	0	StrCC(41)+bendHCC(23)
26	1313(m)	1390	1316	6	0	StrCC(39)+bendHCC(21)
27		1372	1298	14	1	bendHCC(38)
28		1350	1277	3	3	bendHCC(31)
29		1334	1262	1	4	StrCC(53)
30	1255(s)	1326	1255	19	0	StrCC(35)
31		1322	1251	5	7	StrCC(37)+bendHCC(34)
32	1238(s)	1309	1238	36	1	StrCC(44)+bendHCC(25)
33		1290	1221	49	4	StrCC(15)+StrOC(40)
34	1184(w)	1253	1186	72	10	StrCC(30)+bendHCC (10)
35		1236	1169	26	7	Strcc(15)+bendHCC (34)
36		1204	1139	1	3	bendHCH(11)+TorsHCOC(48)
37	1130(m)	1202	1137	1	4	bendHCC(27)
38		1189	1125	83	0	StrCC(15)+bendHCC (27)+bendCCC(11)
39	1093(m)	1160	1098	0	9	bendHCH(28)+TorsHCOC(72)
40	1058(m)	1120	1060	2	0	StrCC(10)+bendHCC(33)
41		1135	1074	3	0	StrCC(25)+bendHCC(54)
42		1107	1048	26	0	StrCC(49)+Cl-C(16)
43	1010(m)	1078	1020	15	0	StrCC(10)+StrOC(72)
44		1055	999	14	11	bendCCC(39)+bendCCC(41)
45		1026	971	14	0	bendHCC(36)+bendHCC(10)+bendCCC(40)
46		1022	967	0	0	TorsHCCC(85)

47		1007	953	0	0	TorsHCCC(79)
48		1001	947	7	0	TorsHCCC(83)
49		970	918	0	0	StrCC(20)+bendCCC(41)
50		950	899	0	0	TorsHCCC(65)+TorsCCC(13)
51		947	896	1	0	TorsHCCC(47)+TorsCCCC(13)
52	864(w)	898	850	1	0	TorsHCCC(36)+OUTOCCC(20)
53		873	826	0	0	StrCC(28)+bendCCC(19)
54	813(m)	858	812	0	0	TorsHCCC(52)
55		840	795	12	0	TorsHCCC(42)+OUTOCCC(11)
56		816	772	0	0	TorsHCCC(97)
57	765(m)	806	762	6	0	TorsHCCC(64)
58	750(m)	791	749	5	0	StrCC(10)+StrOC(18)
59		771	730	5	1	StrCC(10)+StrCl-C(11)
60		751	710	2	0	TorsHCCC(12)+TorsCCCC(13)+OUTOCOC(19)
61	675(w)	727	688	0	0	TorsCCCC(56)
62		677	641	2	0	TorsCCCC(35)+OUTOCCC(23)
63		674	638	1	0	bendCCC(52)
64		652	616	1	0	bendCCC(68)
65		646	611	1	0	bendOCC(30)
66	595(w)	593	561	5	0	bendOCC(31)
67	520(m)	534	506	12	2	bendOCC(16)+bendCCC(10)+bendCOC(17)
68		524	495	5	0	TorsCCCC(26)+OUTOCCC(30)
69		504	477	1	0	TorsCCCC(43)+OUTCl-CCC(28)
70		480	454	1	0	StrCl-c(12)+bendCCC(25)+bendCOC(15)
71		468	443	2	0	StrCl-C(17)+bendCCC(26)
72	414(w)	423	401	0	0	TorsHCCC(23)+TorsCCCC(62)

73	410	388	0	0	TorsHCCC(13)+TorsCCCC(54)
74	357	338	0	0	TorsHCCC(35)+OUTOCCC(17)
75	344	325	3	0	bendCCC(42)+bendCOC(14)+bendCl-CC(12)
76	327	309	0	0	bendCCC(12)+bendCl-CC(41)
77	313	296	0	0	OUTCl-CCC(33)+OUTCCCC(29)
78	271	256	0	0	bendOCC(38)+bendCOC(29)
79	250	236	0	0	TorsHCOC(70)
80	232	219	0	0	StrCC(18)+bendCCC(14)+bendCl-CC(15)
81	179	170	1	0	TorsCCCC(38)+TorsCOCC(23)+OUTOCCC(10)
82	169	160	0	0	bendCCC(48)+bendCl-CC(11)
83	126	120	0	0	TorsCCCC(26)+TorsCOCC(34)
84	104	98	1	0	TorsCCCC(38)+OUTCl-CCC(12)+OUTCCCC(24)
85	84	80	1	0	TorsCCCC(39)+TorsCOCC(27)
86	70	66	0	0	bendCCC(52)
87	49	46	0	0	TorsCCCC(77)
88	37	35	0	0	TorsCCCC(78)
89	14	13	0	0	TorsHCCC(20)+TorsCCCC(54)
90	-124	-117	0	0	StrCC(32)+bendCCC(16)

[a]Str: Stretching; bend: In Plane bending; Tors: Torsion; OUT: Out-of-plane bending; PED: potential energy distribution.IR intensity (Km mol $^{-1}$), Raman intensity (arb.units)

[b] Scaling factor0.9461for DFT (B3LYP)/6-311++G (d,p)

[c] Relative absorption intenditied normalised with highest absorption peak =100.

[d] Relative Raman intensities normalized to 100.

3.2.2 C-C Vibrations

Vibrations due to C-C bond and C-C ring stretching vibrations appear in the region 1625–1430 cm^{-1}. The IR bands at 1666(m), 1504(s), 1438(m), 1313(m),1255(s), and 1238(m) 1184(w), 1058(m) and 1010(m) cm^{-1} in FTIR spectrum are assigned to aromatic C-C stretching vibrations The calculates frequencies using B3LYP/6-311++G(d,p) for C-C vibrations are 1668 1550, 1536, 1516, 1512, 1460, 1435, 1376, 1346, 1262, 1255, 1551, 1238, 1221, 1208, 1169, 1125, 1077, 1074, 1048, 1020 cm^{-1} (mode no 14, 16, 17, 18, 19, 20, 21, 25, 26, 29, 30, 31, 32, 33, 34, 35, 38, 40, 41, 42, 43) are assigned as C-C stretching vibrations with PED contribution of 48, 24, 56, 49, 46, 10, 10, 41, 39, 53, 35, 37, 44, 15, 30, 15, 15, 10, 25, 49, and 10% respectively.These assignments fit with literature values [29,30].

3.2.3 C = O Vibrations

The carbonyl (C=O) carbon-oxygen double bond is formed by the overlap of pπ-orbitals of carbon and oxygen atom and is highly polar hence, the forceful band observed in the region 1700–1800 cm^{-1}[31]. Also, Koczon' et al. [32,33] observed the C = C and C=O group stretching vibrations in the range 1800-1500 cm^{-1}. Carbonyl Group Vibration molecules are getting highly polar bond containing carbon and oxygen atom which is formed by π-π between carbon and oxygen. Because of the different electronegativity's of carbon and oxygen atoms, the bonding electrons are not equally distributed between the two atoms. In the present study, the band observed at 1583 cm^{-1} in FT-IR for C=O vibration and it coincides with calculated value as 1586, cm^{-1} with a PED minimum contribution. Theses assignments are good agreement with the literature value.

4 NMR Spectral Analysis

Proton and Carbon NMR spectroscopy can provide the significant molecular structural information for the analyses of organic molecule. The reactive ionic species are investigated by frequently using the isotropic chemical shifts. NMR shift values are recognized that precise predictions of molecular structural geometries are vital for reliable reckoning of magnetic properties. The NMR (Experimental^{1}H and^{13}C) spectra were measured by using DMSO solvent are shown in Figs.4 and 5. The theoretical NMR spectral dates were carried out in DMSO solvent. The ^{13}C and ^{1}H NMR chemical shifts (experimental and theoretical) values are listed in Table.3 and NMR spectra of 4MCPO are shown in Figs.4 and 5. The chemical shift values (experimental and theoretical) for ^{13}C and ^{1}H NMR of the 4MCPO compound are given in Table 3. [34]. reported ^{13}C spectral data of organic molecule usually present above 100. In the present work, the 1H NMR chemical shift values of title molecule varying from 7.978 to 3.487 ppm and ^{13}C NMR chemical shift values are observed from 189.6974 to 44.7135ppm. Theoretical ^{13}C and ^{1}H NMR chemical shift values well coincides with the experimental values.

` In this work, the ^{13}C chemical shift vales of aromatic ring in 4MCPO molecule is C_5, C_6, C_7, C_8, C_9, C_{10}, C_{11}, C_{12}, C_{13}, C_{14}, C_{16} and C_{17} atoms (exp./cal. in DMSO-d_6 solvent) at the intervals 121.52/121.32-126.91/126.73-126.64/126.28. The C_1 atom which is connected to the electronegative O_4 oxygen atom of the carbonyl group of 4MCPO has the highest chemical shift value (exp./cal.) as 189.16/189.69ppm. Likewise, the methyl group C_{19} atom is present lowest chemical shift value (exp./cal.) at 44.82/44.71ppm (Table 3). As for the chemical shift values of the hydrogen atoms in 4MCPO molecule of methyl group is H_{30} , H_{31} and H_{32} atoms have the lowest values (exp./cal.) as 4.015/4.0426,-3.998/4.038 and 3.477/3.4039 ppm. For other hydrogen atoms, proton chemical shift values (exp./cal.) take place at the interval 7.946/7.978- 7.257/7.282ppm. The observed chemical shift values are good agreement with the calculated values both carbons and protons NMR spectra of 4MCPO molecule.

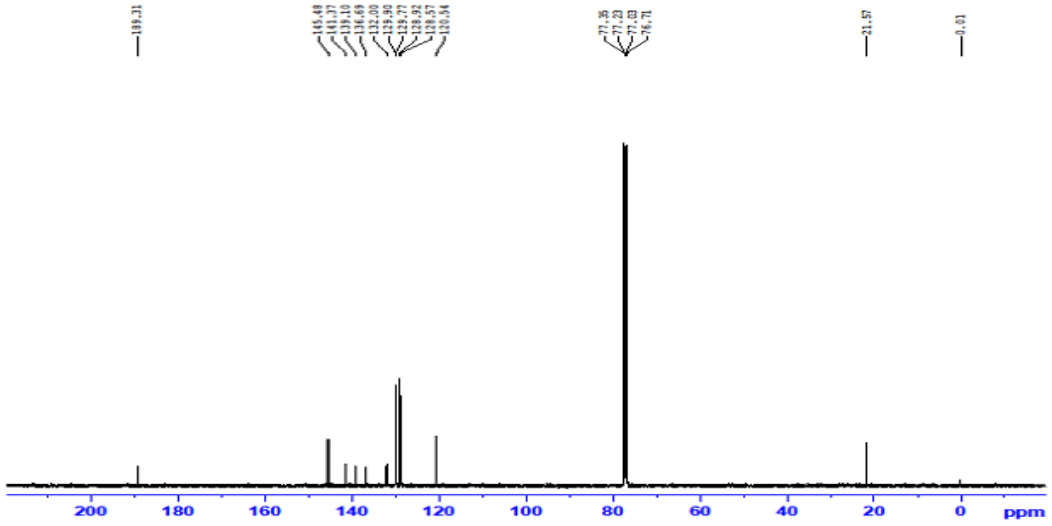

Fig. 4. ^{13}C NMR spectrum of 4MCPO (Experimental)

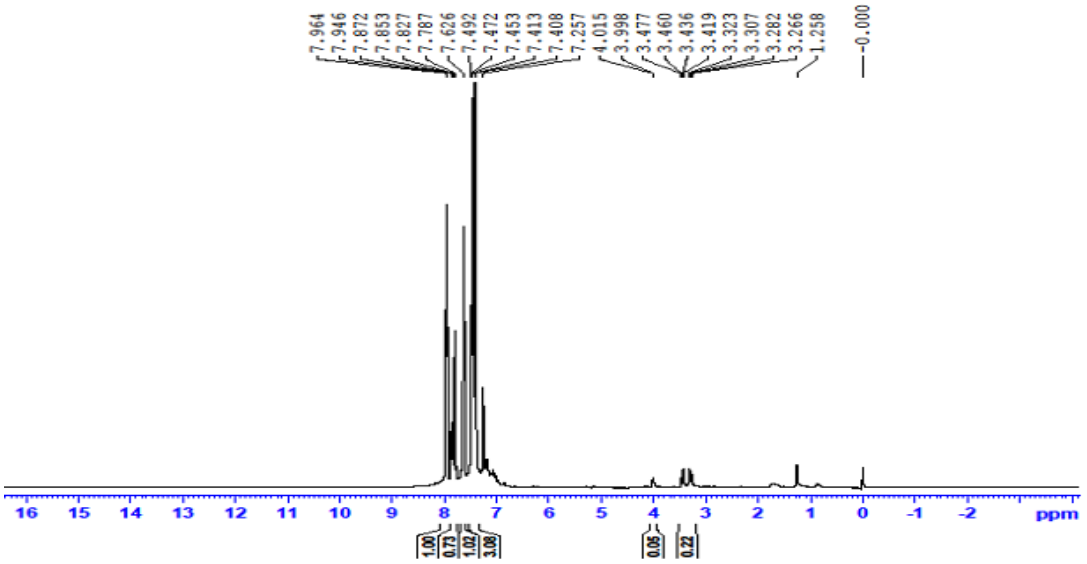

Fig. 5. ^{1}H NMR spectrum of 4MCPO. (Experimental)

Table.3 Theoretical and experimental ^{13}C and ^{1}H isotropic chemical shifts [with respect to TMS, all values in ppm] for 4MCPO molecule

		chemical shifts (ppm)			
Atom	Experimental	B3LYP/6-311++G(d,p)	Atom	Experimental	B3LYP/6-311++G(d,p)
C_1	189.16	189.6974	H_{20}	7.946	7.9501
C_2	121.52	121.3214	H_{21}	7.964	7.978
C_3	145.36	145.2687	H_{22}	7.853	7.864

C_5	136.53	136.8595	H_{23}	7.408	7.4846
C_6	126.91	126.7346	H_{24}	7.257	7.2826
C_7	126.64	125.2822	H_{25}	7.853	7.8831
C_8	139.69	138.8551	H_{26}	7.626	7.8901
C_9	129.77	129.0099	H_{27}	7.492	7.581
C_{10}	139.24	139.0922	H_{28}	7.453	7.7726
C_{12}	127.42	127.9308	H_{29}	7.872	7.954
C_{13}	130.77	130.7429	H_{30}	4.015	4.0426
C_{14}	143.45	143.5787	H_{31}	3.998	4.0384
C_{15}	77.35	107.6815	H_{32}	3.477	3.487
C_{16}	130.52	130.7327			
C_{17}	77.23	78.5499			
C_{19}	76.71	76.7135			

5 Electronic Properties

The observed and computed UV-Visible comparison spectrum of title molecule is shown in Fig. 6 Absorption maximum (λ_{max}) of our title molecule is calculated by TD-DFT/B3LYP method with 6-311++G(d,p) basis set. The calculation of molecular orbital geometry shows that the visible absorption maxima of the 4MCPO resemble the electronic transition from HOMO to LUMO. The experimental UV-Vis spectra of 4MCPO molecule were used to DMSO solvent and theoretical calculations were carried out in the DMSO solvent.

The electronic transition amid frontier orbitals such as transformation from HOMO to LUMO as can be seen through the UV-Vis spectra absorption values 302 (Experimental), 303 (DMSO) (Theoretical) are listed in Table 4. The calculated results involving the wavelength, and oscillating strength and band gap energy are carried out compared with experimental data. The band gap energy was calculated using the formula, E = hc/λ. Here h and c are constant; λ is the cut off wavelength. HOMO and LUMO is related to the ionization potential and electron affinity. The energy difference between HOMO and LUMO orbits is called as band gap that is important stability for structure [35,36]. The electronic absorption corresponds that is mainly described by one electron excitation from HOMO to LUMO for these values increase molecular becomes more stable and decreases the intermolecular charge transfer which makes the compound be NLO active. The HOMO and LUMO energies, the energy gap (ΔE), the ionization potential (I), the electron affinity (A), the absolute electronegativity (χ), the absolute hardness (η) and softness (S) for the 4MPPO molecule have been calculated at B3LYP/6-311++G(d,P) basis set (Fig 7) and the result are given in the Table 5.

By using HOMO and LUMO energy values for a molecule, electronegativity and chemical hardness can be calculated as follow:

$$\chi = \frac{I+A}{2} \text{ (Electronegativity)} \quad (5.1)$$

$$\mu = -\frac{(I+A)}{2} \text{ (Chemical potential)} \quad (5.2)$$

$$\eta = \frac{I-A}{2} \text{ (Chemical hardness)} \quad (5.3)$$

s=1/2η (chemical softness), ω=μ²/2η (Electrophilicity index)

Where I and A are ionization potential and electron affinity; I = − E_{HOMO} and A = − E_{LUMO} respectively [37]. Energy gap of title molecule is calculated experimentally by UV-Visible spectrum is 4.1163 eV, Energy gap is calculated theoretically by TD-DFT (DMSO) method is 4.1057 and from HOMO-LUMO diagram is 3.792 eV. All are very well executed which are listed in Table 4 and 5.

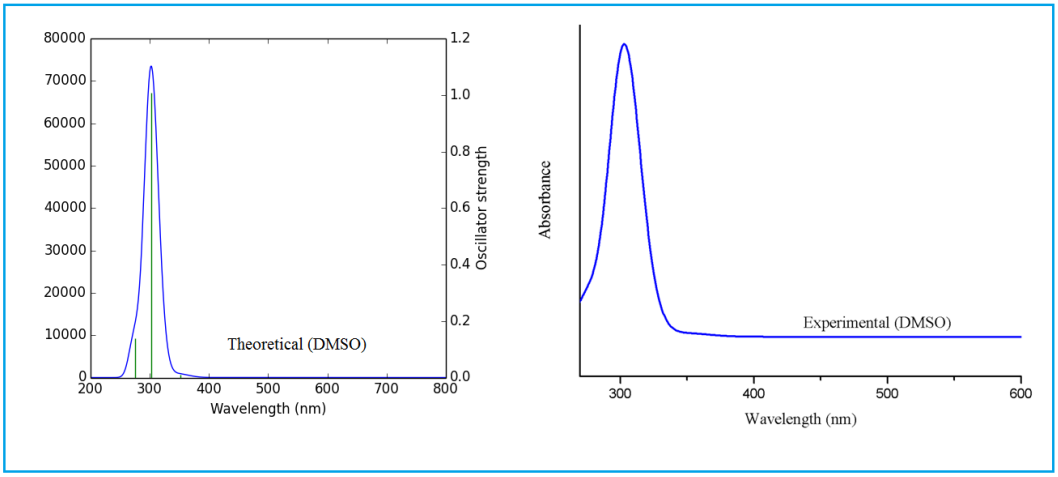

Fig.6. UV–Vis spectra of 4MCPO (Experimental, Theoretical (DMSO))

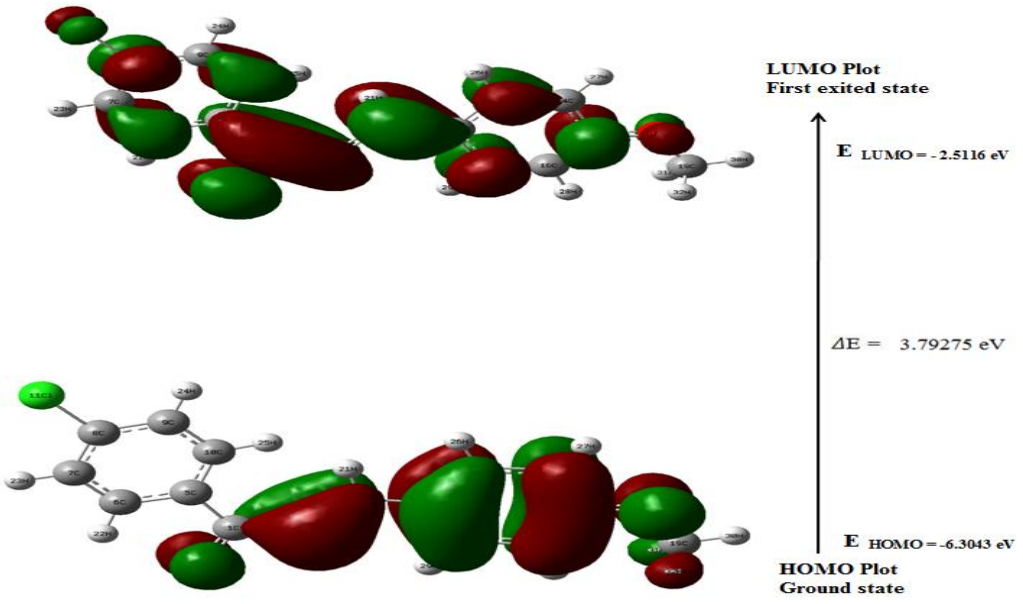

Fig.7 Atomic orbital HOMO – LUMO composition of the frontier molecular orbital for 4MCPO

Table 4 The UV–vis wavelength (λ), band gap energy E (eV), and oscillator strength (f) for 4MCPO calculated by TD-DFT/B3LYP method

Experimental		TD-DFT/B3LYP-311++G(d,p)		DMSO		
λmax (nm)	Bandgap (eV)	λmax (nm)	Bandgap (eV)	Energy (cm^{-1})	Osc. Strength(f)	Assignment Major contributes
—	—	351	3.5384	28464	0.0111	
302	4.1163	303	4.1057	33028	1.0091	HOMO->LUMO (85%)
274	4.5369	275	4.5144	36315	0.1404	H-1->LUMO (86%)

Table 5. Calculated energy values of 4MCPO by B3LYP/6-311++G (d, p)

Basis set	B3LYP/6-311++G(d, p)
HOMO(eV)	-6.30438
LUMO(eV)	-2.51163
Ionization potential	6.30438
Electron affinity	2.51163
Energy gap(eV)	3.79275
Electronegativity	4.40800
Chemical potential	-4.40801
Chemical hardness	1.89637
Chemical softness	0.26366
Electrophilicity index	5.12306

6 Molecular Electrostatic Potentials (MEP)

MEP of 3-(4-methoxy phenyl)-1-(4-chlorophenyl) prop-2-ene-1-one (4MCPO) was calculated using B3LYP/6-311++G(d,p) and to study about electron distribution of molecules. The visual method provides to understand the reaction between structure and the active site of the molecule. It is used to identify the electrophilic and nucleophilic reactivity site and also hydrogen bonding interactions [38, 39]. Negative electrostatic potential corresponds to the attraction of proton by concentrated electron density in the molecule (red) and positive electrostatic potential corresponds to the repulsion of a proton by atomic nuclei in the regions of low electron density (blue). Increases in potential are represented by colour in the order of red < orange < yellow < blue. In Figs. 8 and 9. Shows the colour code at the region from 9.888Ev and -9.888eV, the region with negative potential are over the electronegative oxygen atom and hydrogen atoms are presented in the region of positive potential

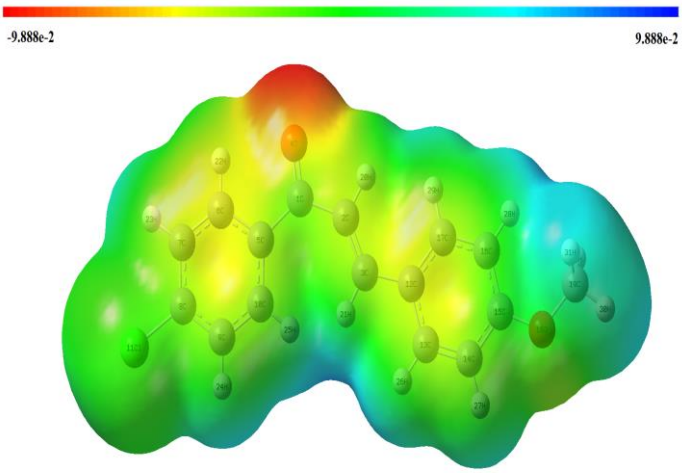

Fig.8 Total electron density mapped with molecular electrostatic potential surface of 4MCPO.

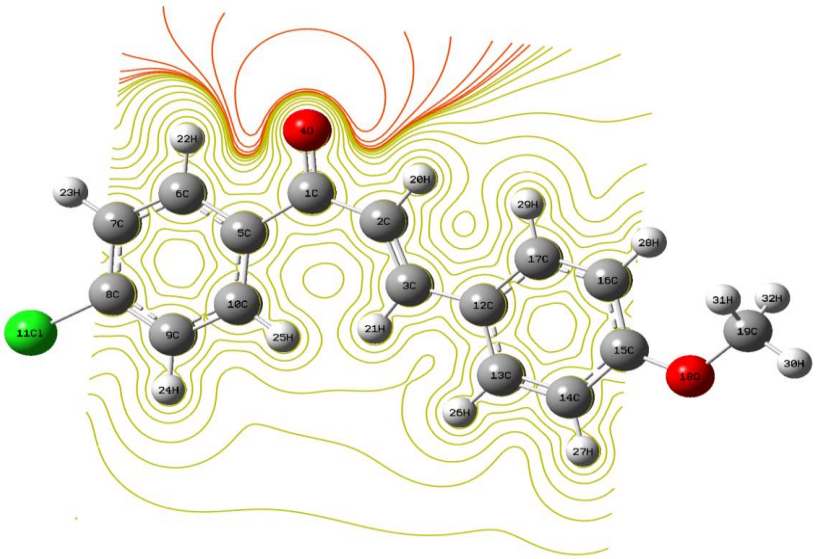

Fig.9. The contour map of electrostatic potential of the total density of 4MCPO.

7 Donor- Acceptor Interactions

The natural bond orbital (NBO) calculations were performed using NBO 3.1 program [40] as implemented in the Gaussian 09 package at the DFT/B3LYP level in order to understand various second-order interactions between the filled orbital of one subsystem and vacant orbital of another subsystem, which is a measure of the intermolecular delocalization or hyper conjugation. NBO analysis provides the most accurate possible 'natural Lewis structure' picture of 'j' because all orbital details are mathematically chosen to include the highest possible percentage of the electron density. A useful aspect of the NBO method is that it gives information about interactions of both filled and virtual orbital spaces that could enhance the analysis of intra and inter molecular interactions. The second-order Fock-matrix was carried out to evaluate the donor–acceptor interactions in the NBO basis.

The strong intra molecular hyper conjugative interaction of C-C to the anti C-C bond of the ring leads to stabilization of some part of the ring as evident from Table.6. For example, in (4MCPO) the π electron delocalization is maximum around C1-O4, C5-C10, C8-C9, C12-C13, C16-C17 distributed to π* antibonding of C2-C3, C1-O4, C5-C10, C2-C3, C14-C15 with a stabilization energy about 9.34, 29.31, 19.97, 24.15, 24.99 kj/mol as shown in Table.6. From σ (C3-H21) to

σ* (C10-H25) with the stabilization energy as 202.28 kj/mol. From σ (C10-H25) to σ* (C3-H21) with stabilization energy of 204.8 kj/mol. And one more important hyper conjugative interactions are LP(1)O4→σ*C1-C5, LP(2)04→σ*(C1-C5) and LP(2)04 → σ*(C2-C3), LP(1) Cl $_{11}$→σ*(C8-C9), LP(2)Cl_{11}→σ*(C7-C8), LP(3)Cl_{11}→σ*(C8-C9), LP(1)O8→σ* (C15-C16) LP(2)O8→σ*(C14-C15) with a stabilization energy about 1.54, 17.02, 0.88, 1.92, 4.34, 13.79, 6.08 and 28.0kj/mol.

Table 6 Second order perturbation theory analysis of fock matrix in NBO basis for 4MCPO

Donor(i)	Type	ED/e	Acceptor(i)	Type	ED/e	[a]E(2) (KJ mol^{-1})	[b]E(J)-E(i) (a.u.)	[c]F(I,j) (a.u.)
C1 -O 4	σ	1.9876	C1-C2	σ*	0.0451	3.55	1.68	0.069
			C1-C5	σ*	0.0638	3.9	1.67	0.073
			C2-C3	σ*	0.0176	1.08	1.71	0.038
			C5-C10	σ*	0.0306	1.7	1.7	0.048
C1 -O 4	π	1.9297	C2-C3	π*	0.1641	9.34	0.4	0.056
			C5-C10	π*	0.3884	8.69	0.4	0.058
C5-C10	σ	1.9624	C5-C6	σ*	0.0330	6.93	1.37	0.087
			C9-C10	σ*	0.0246	5.81	1.38	0.08
			C1-O4	σ*	0.0201	3.24	1.38	0.06
C5-C10	π	1.6355	C1-O4	π*	0.2637	29.31	0.31	0.087
			C6-C7	π*	0.2857	21.67	0.32	0.076
			C8-C9	π*	0.3897	22.89	0.3	0.074
C8-C9	σ	1.9714	C7-C8	σ*	0.0330	5.86	1.41	0.081
			C9-C10	σ*	0.0246	6.1	1.41	0.083
			C7-H23	σ*	0.0189	2.92	1.17	0.052
C8-C9	π	1.6597	C5-C10	π*	0.3884	19.97	0.33	0.074
			C6-C7	π*	0.2857	19.18	0.33	0.072
C12-C13	σ	1.9567	C3-C12	σ*	0.03629	7.64	1.38	0.092
			C12-C17	σ*	0.0409	7.97	1.36	0.093
			C13-C14	σ*	0.0175	5.13	1.36	0.075
C12-C13	π	1.6058	C2-C3	π*	0.1641	24.15	0.31	0.082

Donor(i)	Type	ED/e	Acceptor(i)	Type	ED/e	[a]E(2) (KJ mol^{-1})	[b]E(J)-E(i) (a.u.)	[c]F(I,j) (a.u.)
			C14-C15	π*	0.3816	20.74	0.3	0.071
			C16-C17	π*	0.3005	22.89	0.31	0.077
C16-C17	σ	1.9696	C3-C12	σ*	0.0362	3.47	1.39	0.062
			C12-C17	σ*	0.0409	5.1	1.38	0.075
			C15-C16	σ*	0.0336	5.98	1.36	0.081
			C15-O18	σ*	0.0371	4.33	1.11	0.062
C16-C17	π	1.7006	C12-C13	π*	0.4129	19.47	0.32	0.073
	π		C14-C15	π*	0.3816	24.99	0.31	0.08
C3-H21	σ	1.7759	C10-H25	σ*	0.1960	202.28	1.31	0.463
			C2-H20	σ*	0.0290	4.32	0.85	0.057
			C3-H21	σ*	0.1997	23.48	1.31	0.157
C10-H25	σ	1.7747	C10-H25	σ*	0.1960	23.46	1.3	0.157
			C3-H21	σ*	0.1997	204.8	1.3	0.463
			C5-C6	σ*	0.0330	4.04	1.06	0.061
O4	LP (1)	1.9803	C1-C2	σ*	0.0451	1.45	1.3	0.039
			C1-C5	σ*	0.0638	1.54	1.29	0.04
O4	LP (2)	1.9203	C1-C2	σ*	0.0451	15.26	0.87	0.104
			C1-C5	σ*	0.0638	17.02	0.86	0.109
			C2-C3	σ*	0.0176	0.88	0.9	0.026
			C5-C10	σ*	0.0306	0.62	0.9	0.021
			C6-C7	σ*	0.0202	0.6	0.9	0.021
Cl11	LP (1)	1.9916	C7-C8	σ*	0.0330	1.85	1.57	0.048
			C8-C9	σ*	0.0374	1.92	1.55	0.049

Donor(i)	Type	ED/e	Acceptor(i)	Type	ED/e	[a]E(2) (KJ mol^{-1})	[b]E(J)-E(i) (a.u.)	[c]F(I,j) (a.u.)
Cl11	LP (2)	1.9724	C7-C8	σ*	0.0330	4.34	0.97	0.058
			C8-C9	σ*	0.0374	4.2	0.94	0.056
Cl11	LP (3)	1.9187	C8-C9	π*	0.3897	13.79	0.35	0.067
O18	LP (1)	1.9626	C14-C15	σ*	0.0265	0.64	1.18	0.024
			C15-C16	σ*	0.0336	6.08	1.16	0.075
			C19-H30	σ*	0.0110	3.13	0.89	0.047
			C19-H31	σ*	0.0201	0.84	0.88	0.024
			C19-H32	σ*	0.0201	0.85	0.88	0.024
O18	LP (2)	1.8335	C14-C15	π*	0.3816	28	0.36	0.095
			C19-H31	σ*	0.0201	5.83	0.67	0.058
			C19-H32	σ*	0.0201	5.83	0.67	0.058

[a]E(2) means energy of hyper conjugative interaction (stabilization energy)

[b]Energy difference between donor and acceptor i and j NBO orbitals.

[c]F(i,j) is the Fock matrix element between i and j NBO orbitals

8 Hyperpolarizability Calculations

The first order hyperpolarizability (β_{total}) of this novel molecular system the related properties (μ, α and Δα) of 4MCPO were investigated by DFT/ Becke-3-Lee-Yang-Parr method with 6-311++G(d,P) basis set, is based on the finite-field approach. Non-linear optical (NLO) is the forefront of present research because of its significance in grants the key functions of frequency shifting, optical modulation, optical switching, optical logic, and optical memory for the emerging technologies in areas such as telecommunications, signal processing, and optical interconnections [41]. Hyperpolarizability are very sensitive to the basis sets and level of theoretical approach employed [34-36], that the electron correlation can change the value of hyperpolarizability.

The non-linear optical response of an isolated molecule in an electric field E_i (ω) can be represented as a Taylor series enlargement of the total dipole moment, μ_{tot}, induced by the field:

$$\mu_{tot} = \mu_0 + \alpha_{ij}E_j + \beta_{ijk}E_jE_k + \ldots, \quad (5.4)$$

where α is the linear polarizability, μ_0 is the permanent dipole moment and β_{ijk} are the first hyperpolarizability tensor components. The isotropic (or average) linear polarizability is defined as:

$$\alpha = \frac{\alpha_{xx} + \alpha_{yy} + \alpha_{zz}}{3} \quad (5.5)$$

The first order hyperpolarizability is a third rank tensor that can be described by 3×3×3 matrix. The 27 components of 3D matrix can be abridged to 10 components owing to the Kleinman symmetry [42]

.Components of the first hyperpolarizability can be reckoned using the following equation:

$$\beta_i = \beta_{iii} + \sum_{i \neq j} (\beta_{ijj} + \beta_{jij} + \beta_{jji}) \quad (5.6)$$

Using the x, y and z components of β, the magnitude of the first hyperpolarizability tensor can be calculated by:

$$\beta_{tot} = \sqrt{(\beta_x^2 + \beta_y^2 + \beta_z^2)} \quad (5.7)$$

The entire equation for reckoning the magnitude of β from Gaussian 09W program output is given a follows:

$$\beta_{tot} = \sqrt{(\beta_{xxx} + \beta_{xyy} + \beta_{xzz})^2 + (\beta_{yyy} + \beta_{yzz} + \beta_{xxy})^2 + (\beta_{zzz} + \beta_{xxz} + \beta_{yyz})^2} \quad (5.8)$$

The calculations of the total molecular dipole moment (μ), linear polarizability (α) and first-order hyperpolarizability (β) from the Gaussian output have been explained in detail previously [43], and DFT has been widely used as an efficient method to investigate the organic NLO materials [44,45]. In addition, the polar properties of the 4MCPO and urea were computed at the DFT (B3LYP)/6-311++G(d,p) level using Gaussian 09W program package.

Urea is the prototypical molecule utilized in investigating of the NLO properties of the compound. For this reason, urea was used often as a threshold value for comparative purpose. The calculated dipole moment and hyperpolarizability values obtained from B3LYP/6-311++G(d,p) methods are collected in Table.7. The first order hyperpolarizability of 4MCPO with B3LYP/6-311++G(d,p) basis set is 34.5947 x 10^{-30} fifteen times greater than the value

of urea (β_o = 0.6230 x 10^{-30} esu). From the computation, the high values of the hyperpolarizabilities of 4MCPO are probably attributed to the charge transfer existing amid the benzene rings within the molecular skeleton. This is evidence for the nonlinear optical (NLO) property of the molecule.

Table 7 The values of calculated dipole moment□□(D), polarizability (□₀), first order hyperpolarizability (βtot) components of 4MCPO.

Title	Enter Values	Title	Enter Values	Title	Enter Values
β_{xxx}	2333.7214	α_{xx}	357.4753	μ_x	-1.5707
β_{xxy}	2105.6312	α_{xy}	46.1429	μ_y	-1.2178
β_{xyy}	873.2855	α_{yy}	232.5392	μ_z	0
β_{yyy}	334.2501	α_{xz}	-0.0009	**μ(D)**	**1.9876**
β_{zxx}	-0.9067	α_{yz}	-0.0008		
β_{xyz}	-0.7127	α_{zz}	102.9060		
β_{zyy}	0.0023	α_0 (a.u)	230.9735		
β_{xzz}	-29.1864	α_0 (e.s.u)	**3.42303×10^{-23}**		
β_{yzz}	-3.4568	Δα(a.u)	657.2485		
β_{zzz}	0.1320	**Δα (e.s.u)**	**9.74042×10^{-23}**		
βtot (a.u)	4004.3361				
βtot (e.s.u)	**34.5947×10^{-30}**				

9 Fukui Function

Fukui function plays a central role in study of chemical reactivity and selectivity. It indicates the propensity of density to deform at a given position in order to accept or donate electrons which are more prone to undergo a nucleophilic or an electrophilic attack respectively. Fukui functions such as nucleophilic attack, electrophilic attack and radical attack have been calculated [46, 47]. *Fukui functions and local softness for selected atomic sites in 4MCPO have been listed in Table 8. It has been found that MPA schemes predict Cl_{11} has lower f_r^- value indicates the possible* site for electrophilic attack. From Table 8 shows, MPA schemes predict the reactivity order for the electrophilic case as C_5>C_{11}>C_3>H_{18}>C_6 >H_{20} >C_{14} H_{26} >H_{21}> H_{27}> H_{23} >H_{22}>H_{29}>H_{30} >H_{31} >H_{25} >H_{24} >C_{12} >H_{28}> C_9>H_{19}.The calculated f_r^+ values predicts that the possible sites for nucleophilic attack C_{13}>C_{10}>C_8>C_{17}>C_7>C_1>C_{16}>C_{15}>C_2 site. The title compound more electrophilic attack than nucleophilic attack. These results show 4MCPO. Compound act as more biological activity.

Table. 8. Condensed fukui function f_r and new descriptor $(sf)_r$ for 4MCPO.

Atoms	f_r^+	f_r^-	f_r^0	$s_r^+ f_r^+$	$s_r^- f_r^-$	$s_r^0 f_r^0$
C_1	-0.1134	0.0126	-0.0504	-0.0237	0.0026	-0.0105
C_2	0.0457	-0.0274	0.0092	0.0096	-0.0057	0.0019
C_3	-0.1118	-0.042	-0.0769	-0.0234	-0.0088	-0.0161
O_4	-0.1353	-0.0816	-0.1085	-0.0283	-0.0171	-0.0227
C_5	0.0323	-0.0439	-0.0058	0.0067	-0.0092	-0.0012

C_6	-0.0384	-0.0134	-0.0259	-0.008	-0.0028	-0.0054
C_7	-0.0284	-0.0204	-0.0244	-0.0059	-0.0043	-0.0051
C_8	0.0637	0.0515	0.0576	0.0133	0.0108	0.012
C_9	-0.0422	-0.0393	-0.0408	-0.0088	-0.0082	-0.0085
C_{10}	-0.0333	0.0033	-0.015	-0.007	0.0007	-0.0031
Cl_{11}	-0.1138	-0.1101	-0.112	-0.0238	-0.023	-0.0234
C_{12}	-0.0076	-0.0395	-0.0236	-0.0016	-0.0083	-0.0049
C_{13}	-0.0082	-0.0247	-0.0164	-0.0017	-0.0052	-0.0034
C_{14}	0.0258	0.0037	0.0147	0.0054	0.0008	0.0031
C_{15}	-0.0146	-0.0117	-0.0132	-0.0031	-0.0024	-0.0028
C_{16}	-0.0272	-0.0591	-0.0432	-0.0057	-0.0124	-0.009
C_{17}	-0.0645	-0.0267	-0.0456	-0.0135	-0.0056	-0.0095

10 Antimicrobial Activity

The title compound was screened for its antimicrobial activity against bacterial and fungal strains by Kirby–Bauer agar well diffusion method [48]. The activity was determined by measuring the inhibition zone diameter values (mm) of the investigated compound and antimicrobial activity of 4MCPO against bacterial and fungal pathogens are shown in Fig.10 and 11. The antimicrobial and solvent sensitivity tests for both bacterial and fungal strains were observed and listed in Table.9 and 10 respectively. It is noted that the DMSO solvent, it has no activity on the microbes. 4MCPO dissolved at two concentrations(100 µl and 200 µl) were screened for their antibacterial activity against four bacterial strains such as, *Enterobacter, Bacillus subtillis, Escherichia coli* and *Klebsiella pneumoniae* and three fungal strains such as, *Candida albicans, A.niger* and *A.fumicatus* which were selected for the present investigation by the agar well diffusion method. From Tables.9 and 10. shows a good activity of 4MCPO against the two bacterial strains Bacillus subtillis and *Klebsiella pneumoniae* and the three fungal strains *Candida albicans,A.nigerandA.fumicatus*.Moreover,it is found that synthesized compound exhibits higher antifungal activity than antibacterial activity and the highest activity is against Candida albicans where *C. albicans* is the most commonly isolated species which can cause infections (Candidiasis or thrush) in humans and other animals.

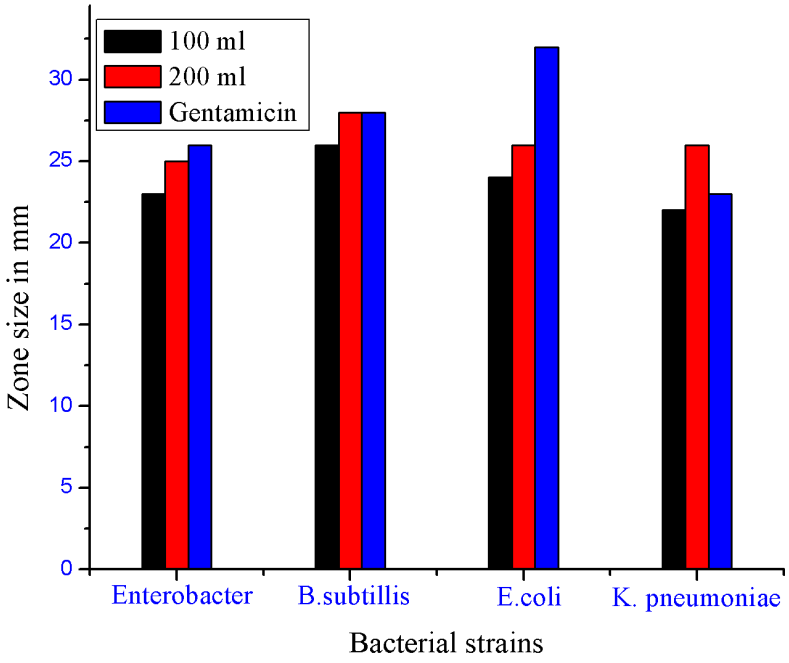

Fig. 10. A bar diagram for the antibacterial activity of 4MCPO

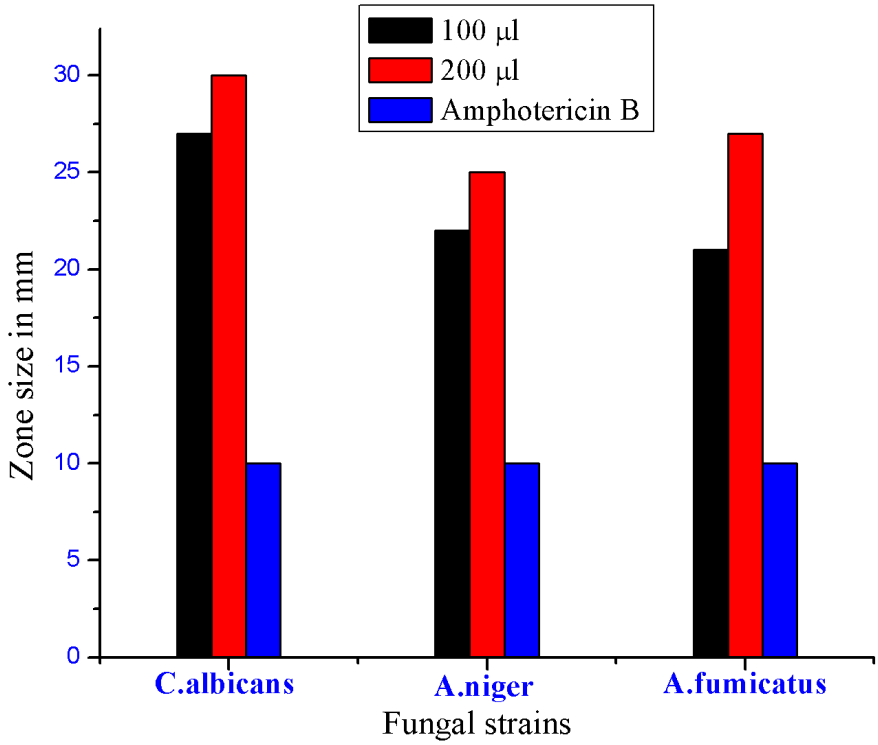

Fig. 11. A bar diagram for the antifungal activity of 4MCPO

Table.9.Antibacterial activity of DMSO extracts

S. no	Bacterial pathogen	DMSO Extract added and Zone of inhibition (mm/ml)			
		100 ml	200 ml	DMSO	Gentamicin
1	Enterobacter	23	25	-	26
2	Bacillus subtillis	26	28	-	28
3	E.coli	24	26	-	32
4	K. pneumoniae	22	26	-	23

Table.10. Antifungal activity of DMSO extracts

S. no	Fungal pathogen	DMSO Extract added and Zone of inhibition (mm/ml)			
		100 ml	200 ml	DMSO	Amphotericin B
1	Candida albicans	27	30	-	10
2	A.niger	22	25	-	10
3	A.fumicatus	21	27	-	10

11 Molecular Modeling Analysis

Auto Dock is a collection of automated docking tools arrange to predict how miniature scale molecules, such as substrates or drug candidate, bind to a receptor of known three dimensional structure. With the aim to investigate the binding mode, a molecular modelling study was performed using Auto Dock Tools for docking 4MCPO. was selected to be docked into the active site of three receptors 4HOE[49], 1QMF[50],3QNJ[51], and 3GFX[52] of antimicrobial proteins which was downloaded from RCSB protein data bank (http: //www. rcsb. org/ pdb/ home/ home .do). In order to examine more comprehensive visualization of potentially fit ligands, Accelrys, Discovery Studio Visualizer 4.1 was utilize for the evaluation of hydrogen bonds in protein-ligand interaction. The ligand was docked into the functional sites of the respective proteins individually and the docking energy was examined to achieve a minimum value. Auto Dock results indicate the binding position and bound conformation of the (CO=NH) peptide, together with a rough estimate of its interaction. Docked conformation which had the lowest binding energy was chosen to investigate the mode of binding. The molecular docking binding energies (kcal/mol) and inhibition constants (μm) were also obtained and listed in Table.11. Among them, 4HOE exhibited the lowest free energy at -7.95 kcal/mol and most docked inhibitors interacted with the ligand within the 4HOE binding site. They exhibited up to two N H...O hydrogen bonds involving ARG56, ILE96 with RMSD being 35.42A^0. The docking simulation shows the binding mode of the 4MCPO into 4HOE. The 4MCPO ligand interacts with different receptors are shown in Fig.12 and 13.

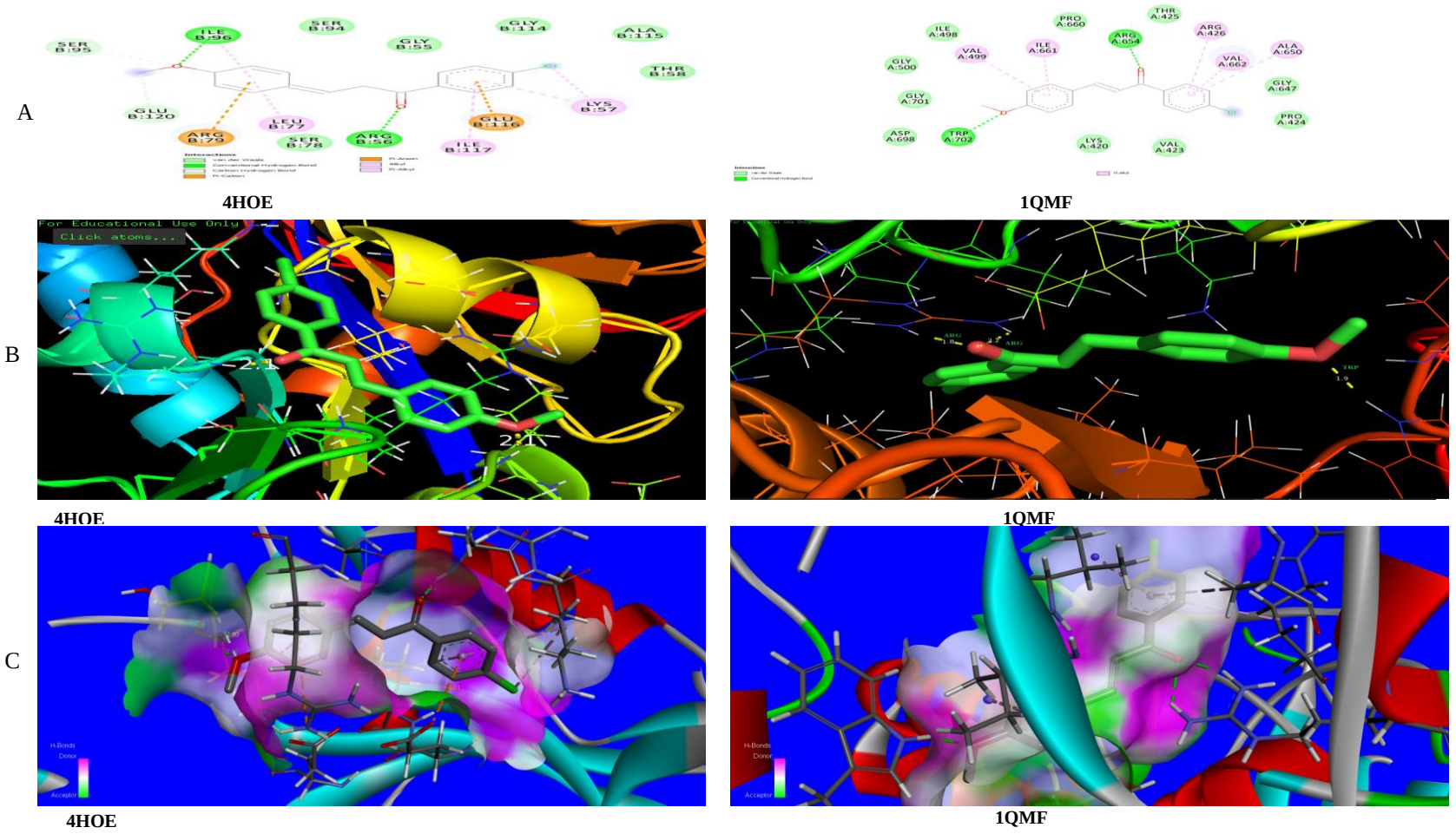

Fig. 12. (a) 4MCPO interaction (2D), (b) and (c) 4MCPO docked into the binding site (3D), 4HOE and 1QMF

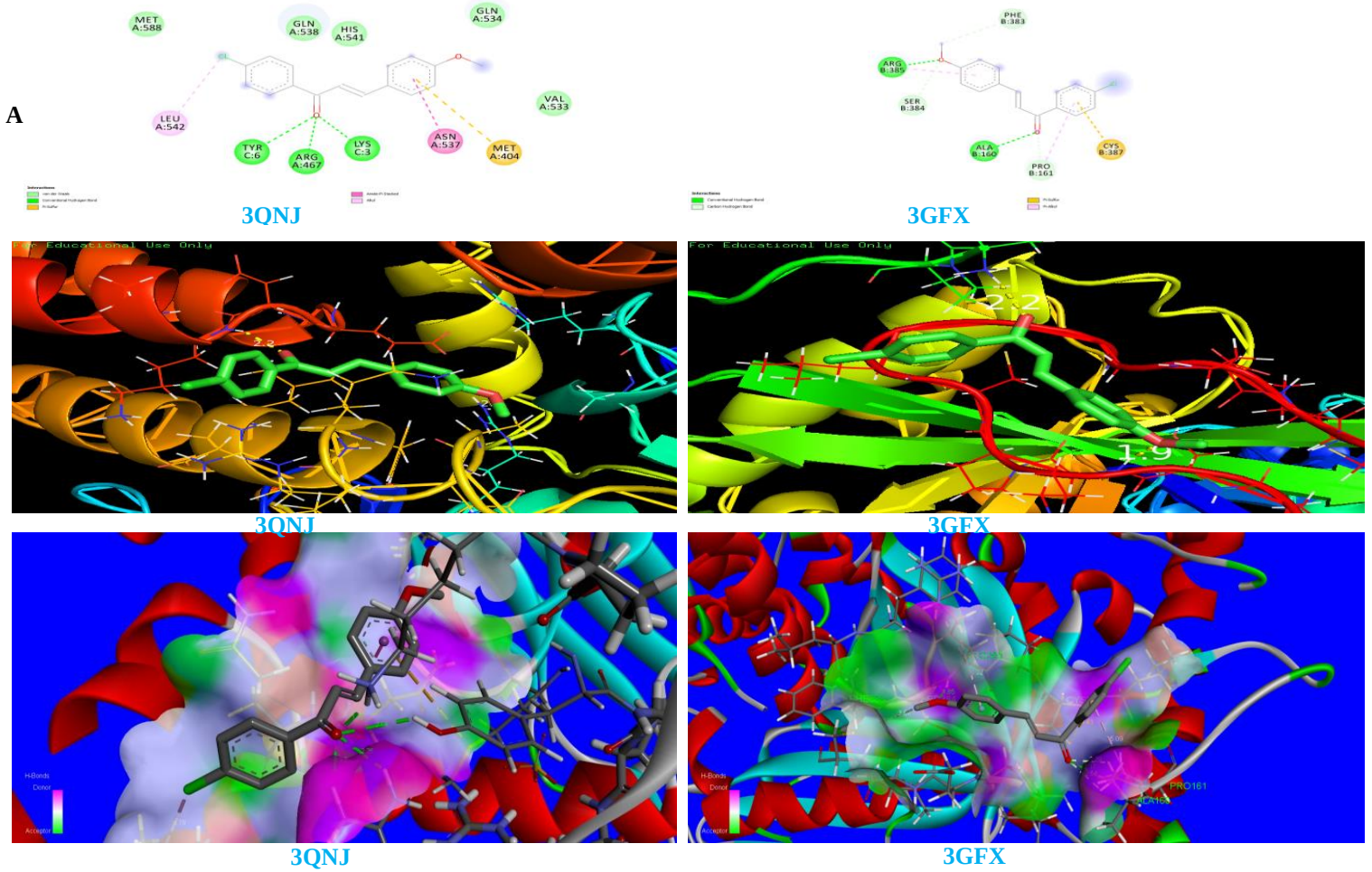

Fig. 13. (a) 4MCPO. interaction (2D), (b) and (c) 4MCPO. docked into the binding site (3D), 3QNJ and 3GFX'

Table.11. Hydrogen bonding and molecular docking with antimicrobial protein targets.

Protein (PDB ID)	Bonded residues	Binding energy (Kcal/mol)	No.of hydrogen bond	Bond distance(A^0)	Estimated Inhibition Constant(μm)	Reference RMSD(A^0)	Torsional energy
4HOE	ARG 56:HN	-7.95	2	2.1	1.48	35.42	1.19
	ILE 96:HN			2.1			
1QMF	ARG654:HH12	-7.44	3	2.2	3.53	136.64	1.19
	ARG654:HH22			1.8			
	TRP702:HE1			1.9			
3QNJ	ARG 447:NH21	-5.95	2	2.2	43.52	16.4	1.19
	LYS 581:HN			2			
3GFX	ALA 160:HN3	-4.84	2	2.2	281.95	38.42	1.19
	ARG 385:HN			1.9			

12 Thermodynamic Properties

Standard statistical thermodynamics function, heat capacity $\left(C^{0}_{p,m}\right)$, entropy $\left(S^{0}_{m}\right)$ and enthalpy changes $\left(H^{0}_{m}\right)$ were computed at B3LYP/6-311++G(d,p) basis set by using perl script THERMO.PL [53] and are listed in Table 12. Thermodynamic functions are all values increasing with temperature ranging from 100 to 1000K due to the fact that the molecular vibrations intensities increase with temperature.

The correlation equation among heat capacities, entropies, enthalpy changes with temperatures were fitted by quadratic formulas and the corresponding fitting factors (R^2) these thermodynamic properties are 0.9999, 0.9999 and 0.9999 respectively. The correlations plot of those shown in Fig 14.

The thermodynamic correlation fitting equation is follows:

$\left(S^{0}_{m}\right)$, =257.02+0.8951T-1.8571T^2X10^{-4}; (R^2 = 0.9999), (5.9)

$\left(C^{0}_{p,m}\right)$ = 2.8163+0.8896T-3.726 T^2X10^{-4}; (R^2 = 0.9999), (5.10)

$\left(H^{0}_{m}\right)$ = -9.278+0.0960T+2.4213 T^2X10^{-4}; (R^2 = 0.9999), (5.11)

All thermodynamic data provide useful information for further studies. They can be used to compute other thermodynamic energies according to relationships of thermodynamic functions and estimate directions of chemical reactions according to the second law of thermodynamics in thermo chemical field [54].

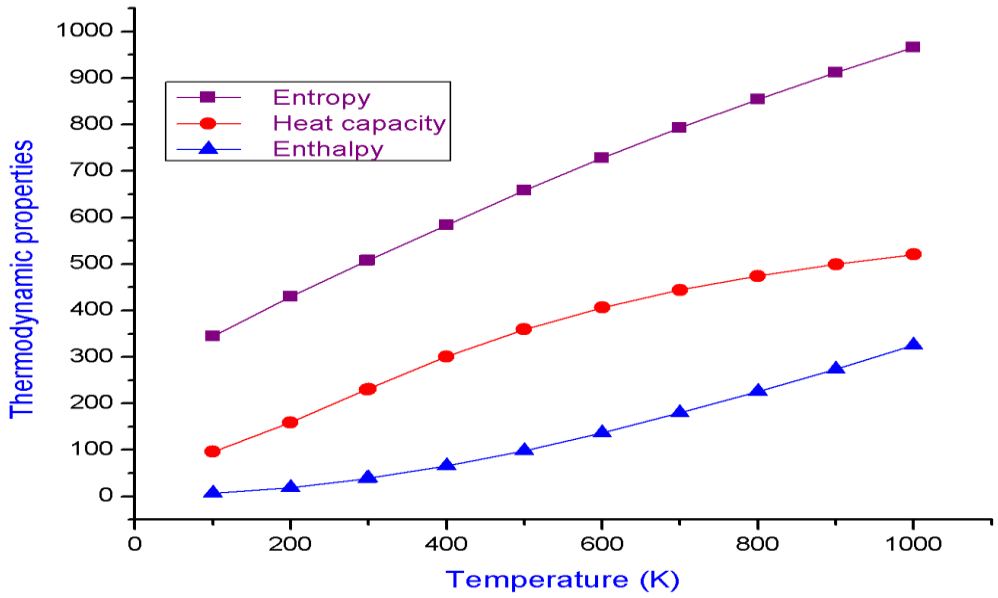

Fig.14 Correlation plot of thermodynamic properties at different temperature of the 4MCPO compound

Table. 12 Thermodynamic properties for 4MCPO obtained by B3LYP/6-311++G(d,p) method

Temp (K)	S^{0}_{m} (J/mol.K)	$C^{0}_{p,m}$ (J/mol.K)	H^{0}_{m} (kJ/mol)
100	344.861	96.1	6.633

200	429.974	158.894	19.271
298.15	506.572	230.156	38.333
300	508	231.51	38.76
400	584.329	300.999	65.459
500	658.001	359.456	98.583
600	727.844	406.353	136.962
700	793.406	443.873	179.541
800	854.732	474.309	225.501
900	912.091	499.397	274.225
1000	965.825	520.355	325.243

13 Conclusions

In the present work, the optimized molecular structure, thermodynamic and electronic properties, vibrational frequencies, the intensity of vibrations of the title compound are calculated by DFT method using B3LYP/6-311++G(d,p) basis set. The optimized geometric parameters (bond lengths and bond angles) are theoretically determined by DFT theory and compared with the experimental data. The vibrational FT-IR spectram of the 1- (4-Chlorophenyl) -3-Methoxyphenyl) prop-2-em-1-one.(4MCPO.) molecule are recorded and on the basis of agreement between the calculated and experimental results, the assignments of all the fundamental vibrational modes of the title compound are made unambiguously based on the results of the PED output obtained from the normal coordinate analysis. The NBO analysis explained the intra molecular hydrogen bonding and the hyper conjugative interaction in the molecule. The charge delocalization on the molecule is different with different HOMO, LUMO energy levels. Low HOMO–LUMO energy gap value indicates the intramolecular charge transfer inside the molecule. Fukui function helps to identify the electrophilic and nucleophilic nature of a specific site within a molecule. The MEP shows the negative potential sites are on oxygen and chlorine atoms as well as the positive potential sites around the hydrogen atoms. Orbital energy interactions between selective functional groups are analyzed by the density of energy states. The correlations between the statistical thermodynamical and temperature are also obtained. It was seen that the heat capacities, entropies and enthalpies increase with the increasing temperature owing to the intensities of the molecular vibrations increase with increasing temperature. The molecular docking output shows that the lowest binding energy for 4MCPO is −7.95 kcal/mol and most docked inhibitors interacted with the ligand within the 4HOE binding site.

References

[1] B.K. Sarojini, B. Narayana, B.V. Ashalatha, J. Indira, K.G. Lobo, J. Cryst. Growth 295 (2006) 54- 59.

[2] S. Shettigar, G. Umesh, K. Chadrasekharan, B.K. Sarojini, B. Narayana, Optical Materials 30 (2008) 1297-1303.

[3] P. Poornesh, S. Shettigar, G. Umesh, K.B. Manjunatha, K.P. Kamath, B.K. Sarojini, B. Narayana, Optical Materials 31 (2009) 854–859.

[4] J. Indira, P.P. Karat, B.K. Sarojini J. Cryst. Growth 242 (2002) 209-214.

[5] S.F. Nielsen, S.B. Christensen, G. Cruciani, A. Kharazmi, T. Liljefors, J. Med. Chem. 41 (1998) 4819–4832.

[6] C.W. Mai, M. Yaeghoobi, N. Abd-Rahman, Y.B. Kang, M.R. Pichika, Eur. J. Med. Chem. 77 (2014) 378-387.

[7] M. Wan, L. Xu, L. Hua, A. Li, S. Li, W. Lu, Y. Pang, C. Cao, X. Liu, P. Jiao, Bioorg. Chem. 54 (2014) 38-43.

[8] S. Mukherjee, V. Kumar, A.K. Prasad, H.G. Raj, M.E. Bracke, C.E. Olsen, S.C. Jain, V.S. Parmar, Bioorg. Med. Chem. 9 (2001) 337–345.

[9] Y.M. Lin, Y. Zhou, M.T. Flavin, L.M. Zhou, W. Nie, F.C. Chen, Bioorg. Med. Chem. 10 (2002) 2795–2802.

[10] S.N. Lopez, M.V. Castelli, S.A. Zacchino, J.N. Dominguez, G. Lobo, C.C. Jaime, J.C.G. Cortes, J.C. Ribas, C. Devia, M.R. Ana, D.E. Ricardo, Bioorg. Med. Chem. 9 (2001) 1999–2013.

[11] Z.N. Siddiqui, T.N.M. Musthafa, A. Ahmad, A.U. Khan, Bioorg. Med. Chem. Lett. 21 (2011) 2860-2865.

[12] A. Agarwal, K. Srivastava, S.K. Puri, P.M.S. Chauhan, Bioorg. Med. Chem. 13 (2005) 4645-4650.

[13] B. Insuasty, A. Montoya, D. Becerra, J. Quiroga, R. Abonia, S. Robledo, I.D. Velez, Y. Upegui, M. Nogueras, J. Cobo, Eur. J. Med. Chem. 67 (2013) 252-262.

[14] R. Abonia, D. Insausty, J. Castillo, B. Insausty, J. Quiroga, M. Nogueras, J. Cobo, Eur. J. Med. Chem. 57 (2012) 29-40.

[15] V. Sharma, A. Chaudhary, S. Arora, A.K. Saxena, M.P.S. Ishar, Eur. J. Med. Chem. 69 (2013) 310-315.

[16] S. Shenvi, K. Kumar, K.S. Hatti, K. Rijesh, L. Diwakar, Eur. J. Med. Chem. 62 (2013) 435-442.

[17] S. Alen, D. Sajan, L. Joseph, K. Chaitanya, V. Shettigar, V.B. Jothy, Synthesis, growth, vibrational spectral investigations and structure–property relationship of an organic NLO crystal: 3, 4-Dimethoxy chalcone. Chem. Phys. Lett. 636 (2015) 208-215.

[18] M.J. Frisch, G.W. Trucks, H.B. Schlegel, G.E. Scuseria, M.A. Robb, J.R. Cheeseman, G. Scalmani, V. Barone, B. Mennucci, G.A. Petersson, H. Nakatsuji, M. Caricato, X. Li, H.P. Hratchian, A.F. Izmaylov, J. Bloino, G.Zheng, J.L. Sonnenberg, M. Hada, M. Ehara, K. Toyota, R. Fukuda, J. Hasegawa, M. Ishida, T. Nakajima, Y. Honda, O. Kitao, H. Nakai, T. Vreven, J.A. Montgomery, Jr., J.E. Peralta, F. Ogliaro, M. Bearpark, J.J. Heyd, E. Brothers, K.N. Kudin, V.N. Staroverov, R. Kobayashi, J. Normand, K. Raghavachari, A. Rendell, J.C. Burant, S.S. Iyengar, J. Tomasi, M. Cossi, N. Rega, J.M. Millam, M. Klene, J.E. Knox, J.B. Cross, V. Bakken, C. Adamo, J. Jaramillo, R. Gomperts, R.E. Stratmann, O. Yazyev, A.J. Austin, R. Cammi, C. Pomelli, J.W. Ochterski, R.L. Martin, K. Morokuma, V.G. Zakrzewski, G.A. Voth, P. Salvador, J.J. Dannenberg, S. Dapprich, A.D. Daniels, Ö. Farkas, J.B. Foresman, J.V. Ortiz, J. Cioslowski, and D.J. Fox, Gaussian 09, Revision E.01, Gaussian, Inc., Wallingford CT, 2009.

[19] M.H. Jamroz, Vibrational energy distribution analysis (VEDA): scopes and limitations, Spectrochim. Acta A 114 (2004) 220-230.

[20] S. Murugavel, V. Vetri velan, D. Kannan, M. Bakthadoss, Synthesis of a novel methyl(2*E*)-2-{[*N*-(2-formylphenyl)(4-methylbenzene)sulfonamido] methyl}-3-(2-methoxyphenyl)prop-2-enoate:molecular structure, spectral, antimicrobial, molecular docking and DFT computational approaches, , J. Mol. Struct. 1127 (2017) 457–475.

[21] M. Raja, R. Raj Muhamed, S. Muthu, M. Suresh, K. Muthu, Synthesis, spectroscopic (FT-IR, FT-Raman, NMR, UV-Visible), Fukui function, antimicrobial and molecular docking study of (E)-1-(3-bromobenzylidene)semicarbazide, J. Mol. Struct. 1130 (2017) 374–384.

[22] M. Cinar, M. Karabacak , A.M. Asiri, An experimental and density functional study on conformational and spectroscopic analysis of 5-methoxyindole-2-carboxylic acid, Spectrochim. Acta Part A 137 (2015) 670-676.

[23] L.-H. Jing (E)-1-(4-Nitrophenyl)-3-phenylprop-2-en-1-one, Acta Cryst E65, (2009) 2510.

[24] A. Abbas, H. Gokce, S. Bahçeli, M.M. Naseer, Spectroscopic (FT-IR, Raman, NMR and UV–vis.) and quantum chemical investigations of (E)-3-[4-(pentyloxy) phenyl]-1-phenylprop-2-en-1-one. J. Mol. Struct. 1075 (2014)352-364.

[25] N. Swarnalatha, S.Gunasekaran, S. Muthu, M. Nagarajan, Molecular structure analysis and spectroscopic characterization of 9-methoxy-2H-furo[3,2-g]chromen-2-one with experimental (FT-IR and FT-Raman) techniques and quantum chemical calculations, spectrochim. Acta part A 137 (2015) 721-729.

[26] L.G. Wade (Ed), Advanced Organic Chemistry, 4th ed., Wiley, New York,1992. p.723.

[27] M. H. Jamróz, J. Cz. Dobrowolski, R. Brzozowski, Vibrational modes of 2,6-, 2,7-, and 2,3-diiso-propylnaphthalene. A DFT study, J. Mol. Struct. 787, (2006)172–183.

[28] S. Muthu, A. Prabhakaran, Vibrational spectro-scopic study and NBO analysis on

[29] S. Gunasekaran, R. Thilak Kumar, S. Ponnusamy, Vibrational Spectra And Normal Coordinate Analysis Of Diazepam, Phenytoin And Phenobarbitone., Spectrochim. Acta A 65 (2006) 1041–1052.

[30] Vinod Mathew, J.Keshavayya,V.P.Vaidya, Synthesis, characterization and pharmacological activities of 3, 6-disubstituted-1, 2, 4-triazolo [3, 4-b]-1, 3, 4-thiadiazoles and their dihydro analogues. E-J Chem. 4 (2007) 320–342.

[31] Sudha, N. Sundaraganesan, K. Vanchinathan, K. Muthu, S.P. Meenakshisundarm, Spectroscopic (FT-IR, FT-Raman, Nmr And Uv)And Molecular Structure in vestigations Of 1, 5-Diphenylpenta-1, 4-Dien-3-One: A Combined Experimental And Theoretical -J. Mol. Struct. 1030 (2012) 191–203.

[32] Koczon, J.Cz. Dobrowolski, W. Lewandowski, A.P. Mazurek, J. Experimental and theoretical IR and Raman spectra of picolinic, nicotinic and isonicotinic acids.Mol. Struct 655 (2003) 89–95.

[33] Snehalatha M, Ravikumar C, Hubert Joe I, Jayakumar V S, Vibrational spectra and scaled quantum chemical studies of the structure of Martius yellow sodiumsaltmonohydrate,Journal of Raman spectrosc,40 (2009)1121.

[34] R. Ditchfield, Molecular orbital theory of magnetic shielding and magnetic susceptibility,J. Chem. Phys. 56 (1972) 5688-5692.

[35] P. Udhayakalaa , T.V. Rajendran , S. Gunasekaran , Theoritical study using dft calculations on inhibitory action of some pyrazole derivatives on steel, J. Adv. Sci. Res. 4 (2) (2013) 31–37 .

[36] R.G. Pearson, Absolute electronegativity and hardness correelaed with molecular orbital theory, Proc. Natl. Acad. sci. 83 (22) (1986) 84 40–84 41

[37] S. Xavier, S. Periandy, Spectroscopic (FT-IR, FT-Raman, UV and NMR investigation on 1-phenyl-2-nitropropeneby quantum computational calculations, Spectrochim. Acta; Mol. Biomol. Spectrosc. 149 (2015) 216–230.

[38] E. Scrocco, J. Tomasi, Topics in Current Chemistry, vol. 7, Springer, Berlin,1973.

[39] J.S. Murray, K. Sen, Molecular Electrostatic Potentials, Concepts and Applications, Elsevier, Amsterdam, The Netherlands, 1991.

[40] R. Srinivasaraghavan, S. Thamaraikannan, S. Seshadri, T. Gnanasambandan, Molecular conformational stability and spectroscopic analysis of Parared with experimental techniques and quantum chemical calculations, Spectrochim. Acta A 137 (2015) 1194-1205.

[41] G. Velraj, S. Soundharam, C. Sridevi, Structure, vibrational, electronic, NBO and NMR analyses of 3-methyl-2,6-diphenylpiperidin-4-one (MDPO) by experimental and theoretical approach, Journal of Molecular Structure 1060 (2014) 156-165.

[42] A.E. Reed, L.A. Curtiss, F. Weinheld, Intermolecular Interactions from a Natural Bond Orbital, Donor-Acceptor Viewpoint, Chem.Soc. 102 (1988) 899-926.

[43] J.P. Foster, F. Weinhold, Natural Hybrid Orbitals, J. AM. Chem. Soc. 102 (1980) 7211-7218.

[44] H. Sekino, R.J. Bartlett, Hyperpolarizabilities of the hydrogen fluoride molecule: A discrepancy between theory and experiment?, J. Chem. Phys. 84 (1986) 2726-2733.

[45] C. Cassidy, J.M. Halbout, W. Donaldson, C.L. Tang, Nonlinear optical properties of urea, Opt. Commun 29 (2) (1979) 243e247.

[46] R.G. Parr, W. Yang, Functional Theory of Atoms and Molecules, OxfordUniversity Press, New York, 1989.

[47] P. Politzer, P. Lane, A computational study of some nitrofluoromethanes Struct.Chem. 61 (1990) 159-164.

[48] N.T. Abdel-Ghani , M.F.A. El-Ghar, A.M. Mansour, Novel Ni(II) and Zn(II) complexes coordinated by 2-arylaminomethyl-1H-benzimidazole: Molecular structures, spectral, DFT studies and evaluation of biological activity, Spectrochimica Acta A 104 (2013) 134-142.

[49] N.G. Dayanandan, L. Paulsen, K. Viswanathan, S. Keshipeddy, N. Lombardo, W. Zhou, M. Lamb, E. Sochia, J.B. Alverson, D. Priestley, L. Wright, C. Anderson Propargyl-linked antifolates are dual inhibitors of Candida albicans and Candida glabrata, J. Med. Chem. 57 (2014) 2643-2656.

[50] Kuppamuthu Sarojini,H.Krishnan,Molecular Docking Studies Of Some Sulfonamide Derivatives as Pbp-2x Inhibitors as Antibacterial agents Romanian J. Biophys.24-3,(2014) 175–184.

[51] D. Knappe, M. Zahn, U. Sauer, G. Schiffer, N. Strater, R. Hoffmann, Rational Design of Oncocin Derivatives with Superior Protease Stabilities and Antibacterial Activities Based on the High-Resolution Structure of the On cocin-DnaK ChemBioChem12 (2011) 874.

[52] A. Ravi Kumar, G. Sathaiah, A. Chandra Shekhar, K. Raju, P. Shanthan Rao, B. Narsaiah, Y. Kanaka Raju, U.S.N. Murthy, V. Srimai, M. Ramesh,T. Parthasarathy, Synthesis of 6-Fluoro-7-cyclic amino-substituted dicarboxylic acid quinolones and their antibacterial activity, J. HeterocyclChem. 51 (2014) 114-122.

[53] K.K. Irikura, THERMO. PL (National Institute of Standards and Technology), Gaithersburg, MD, 2002.

[54] J.B. Ott, J.B. Goates, Chemical Thermodynamics: Principles and Applications, Academic Press, San Diego, 2000